

Time domain detection of pulsed spin torque damping reduction

Longfei Ye¹, Samir Garzon¹, Richard A. Webb¹, Mark Covington², Shehzaad Kaka², and Thomas M. Crawford¹

¹*Department of Physics and Astronomy and USC Nanocenter,
University of South Carolina, Columbia, SC 29208, USA.*

²*Seagate Research, 1251 Waterfront Place, Pittsburgh, PA 15222, USA.*

Combining multiple ultrafast spin torque impulses with a 5 nanosecond duration pulse for damping reduction, we observe time-domain precession which evolves from an initial 1 ns duration transient with changing precessional amplitude to constant amplitude oscillations persisting for over 2 ns. These results are consistent with relaxation of the transient trajectories to a stable orbit with nearly zero damping. We find that in order to observe complete damping cancellation and the transient behavior in a time domain sampling measurement, a short duration, fast rise-time pulse is required to cancel damping without significant trajectory dephasing.

Spin-polarized electrons passing through a nanoscale ferromagnet (nanomagnet) exert a spin-transfer torque (STT) [1, 2] on the local magnetization. In contrast to external field torques, STT can be largely collinear with the Landau Lifshitz Gilbert damping torque [3], allowing control over damping [4, 5], in addition to driving precession and switching [6, 7]. Spin torque's ability to coherently cancel the damping torque holds great potential for applications of nanopillars in high stability, low-linewidth microwave oscillators [10]. Whereas for ac driven oscillators the linewidth depends directly on damping, linewidths of dc driven oscillators are dominated by trajectory dephasing [5, 8]. Measuring and understanding the effects of damping and dephasing is critical for minimizing oscillator linewidths and maximizing their power output [9]. At low temperatures, time-domain [4] and ferromagnetic resonance (FMR) measurements [5] of spin-valve nanopillars have demonstrated spin torque induced damping reduction. Here, we demonstrate damping cancellation at room temperature by using a pulsed time domain technique: two ultrafast (30 ps) spin torque impulses excite nanomagnet dynamics and the switching probability P_S is measured as a function of relative pulse-pulse delay [11]. Our measurement maps a precessional trajectory to a digital response, either switching or nonswitching. We compare damping cancellation using a 5 ns current pulse and a dc current, and show that the dc current leads to switching and dephasing, preventing complete cancellation of damping. However, the 5 ns pulse, at amplitudes well above the "dc" critical current, can cancel the effective damping and yield coherent dynamics over our maximum time window of 2.2 ns. Our technique allows us to observe the transient dynamics that precede orbit stabilization in the presence of a constant current, and the trajectory dephasing that occurs over a longer timescale.

Spin-valve nanopillar devices with elliptical cross section were fabricated using e-beam lithography and ion milling. The devices are composed of an extended $\text{Ni}_{80}\text{Fe}_{20}$ (20 nm)/ $\text{Co}_{90}\text{Fe}_{10}$ (2 nm) polarizer which provides a large magnetic moment to improve its stability, a 10 nm Cu spacer, and a 3 nm $\text{Co}_{90}\text{Fe}_{10}$ "free" layer or

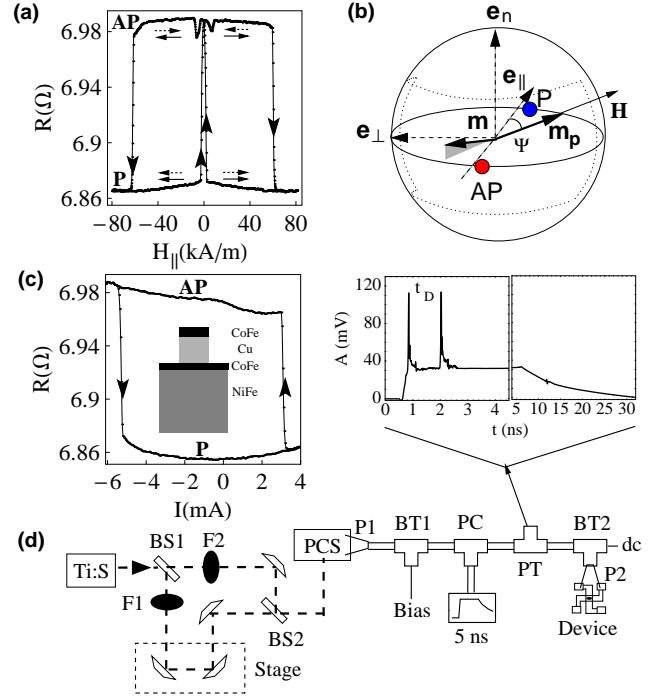


Figure 1: Device characterization and experimental setup. (a) Resistance vs easy-axis magnetic field, $H_{||}$, for a typical device at room temperature. (b) Schematic describing the orientation of the polarizer \mathbf{m}_p and P, AP stable points. \mathbf{m}_p tracks the applied field, H . (c) Resistance vs. dc current for device shown in (a) with $H=46$ kA/m and $\Psi \sim 12$ degrees. Inset: device schematic. (d) Experimental setup for time-resolved measurements of spin torque switching with damping cancellation. Inset: voltage waveform (ultrafast pulse pair plus 5 ns pulse) measured at a pick-off tee before the device.

nanomagnet [Inset to Fig. 1(c)]. A typical plot of resistance vs. field is shown in Fig. 1(a), where the large vertical arrows indicate free layer switching between P and AP states (largely parallel or anti-parallel to the polarizer). The small dashed and solid arrows represent the orientation of the free layer, \mathbf{m} , and polarizer, \mathbf{m}_p , respectively. The measured Stoner-Wohlfarth astroid for our devices indicates that the polarizer follows the applied

field, reversing orientation around zero field [small dips in resistance in Fig. 1(a)]. Polarizer reversal near zero field, along with considerable interlayer dipole coupling, are responsible for the two symmetric loops at positive and negative fields. For all STT measurements we apply an in-plane magnetic field H at a small angle $\Psi \sim 10$ degrees with respect to the easy axis \mathbf{e}_{\parallel} [Fig. 1(b)] to cancel the polarizer's dipolar field, facilitate AP-P current induced switching, and set the orientation of the polarizer to obtain a non-collinear geometry, increasing switching reproducibility [11]. For the values of H used throughout our experiments the orientations of points P and AP are displaced less than 3 degrees from \mathbf{e}_{\parallel} due to the easy axis anisotropy of the free layer. Current, defined as positive when flowing across the multilayer from top to bottom [inset to Fig. 1(c)] can be used to switch the nanomagnet via STT [3]. A typical resistance vs dc current loop [Fig. 1(c)] shows sharp transitions between the P and AP states and a ~ 8 mA wide region of bistability. Four terminal measurements of the P state resistance and magnetoresistance give typical values $\sim 1.6\Omega$ and $\sim 7\%$ respectively. The large two terminal resistance values in Figs. 1(a), (c) are due to lead resistance and inductive impedance of the bias tees shown in 1(d).

To generate ultrafast spin torque current pulses we use an amplified Ti:Sapphire mode-locked laser (120fs FWHM, ~ 1.6 mJ per pulse) in single-shot mode [Fig. 1(d)]. An optical pulse is split into two separate pulses at the first beamsplitter (BS1), with each pulse having independently controlled amplitudes via tunable optical filters (F1, F2). A sub ps resolution variable optical delay t_D between the pulses is produced with a translation stage, after which the beams are recombined at BS2 and focused onto a Au photoconductive switch (PCS) [12]. The two PCS generated electrical pulses (14.9 mA, ~ 30 ps FWHM) are sent through a 40 GHz coplanar-to-coaxial probe (P1) to the PCS bias tee (BT1) with 12 ps risetime and 40V dc switch bias. A power combiner (PC) can add a 25ps risetime, 5 ns duration pulse to the pulse pair, and the resulting signal is then transmitted to the nanomagnet through a 40GHz network which includes a pick-off tee (PT) for pulse monitoring [Fig. 1(d), inset] and a second 40 GHz bias tee (BT2) for injecting dc and low frequency ac currents for device switching and lock-in amplifier measurement of nanopillar resistance. Device connection is made with a second 40GHz coaxial-to-coplanar probe (P2). For each measurement we reset the device to the AP state by using a low frequency current ramp, verify the state of the device by measuring its resistance, send a pair of ultrafast pulses together with either a 5ns duration pulse or a dc current, and measure the final state of the device: P or AP.

The first ultrafast pulse displaces \mathbf{m} away from AP, as indicated by the dark trajectory simulated in Fig. 2(a), and in the absence of spin torque \mathbf{m} relaxes towards AP due to Gilbert damping. As explained in Ref. [11] the white and gray regions are the free precession basins of attraction for P and AP respectively. After some time de-

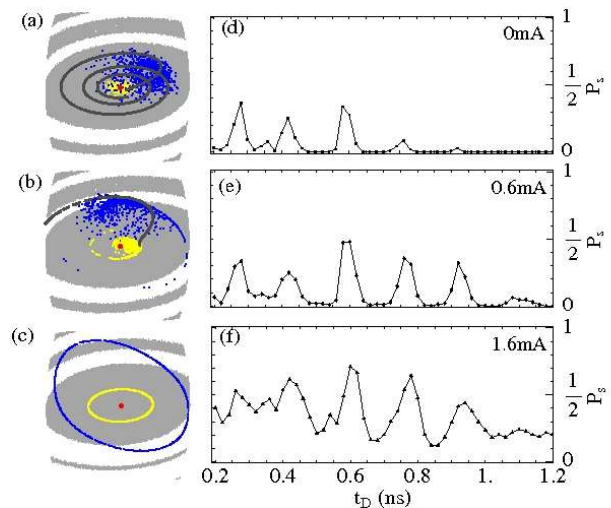


Figure 2: **dc current effective damping reduction** (a)-(c) Sections of the free layer moment phase portrait for the dotted region of Fig. 1(b), without (a, b) and with (c) dc current. Yellow and blue dots represent macrospin simulations of a \mathbf{m} ensemble before and after the (a) first and (b) second ultrafast pulses. The dark line represents a single trajectory (a) before and (b) after the second ultrafast pulse. (c) \mathbf{m} ensemble long after applying a dc current (yellow dots), and same ensemble just after applying the first ultrafast pulse (blue dots). (d)-(f) P_S vs delay between two ~ 30 ps duration pulses for dc currents of (d) 0 mA, (e) 0.6 mA, and (f) 1.6 mA at room temperature. The “dc switching current”, measured using a sweep rate of 0.05 mA/s is ~ 1.8 mA.

lay the second ultrafast pulse displaces \mathbf{m} once again. In the particular case shown in Fig. 2(b) \mathbf{m} ends up inside a white band and thus free evolution of \mathbf{m} leads to switching to the P state. For certain delays, \mathbf{m} can remain within the first gray band or might even be excited into large angle precession gray regions, eventually relaxing towards AP. For every repetition of our experiment the initial orientation of \mathbf{m} will be different due to thermal fluctuations, as indicated by the distribution of yellow dots around the AP state (red) in Fig. 2(a), where every point represents a repetition of the experiment. After the first pulse, the initial \mathbf{m} ensemble shifts to the new one represented by the blue dots in Fig. 2(a). Free evolution transforms it [yellow dots in Fig. 2(b)], and the second pulse pushes the ensemble partially into the first white band [blue dots in Fig. 2(b)], generating a nonzero switching probability for this particular value of delay. By varying the delay we measure the switching efficiency of spin torque at different average orientations of \mathbf{m} . In our experiments we measure hundreds of switching events for each delay to keep the statistical error below 2%. The bandwidth of our technique, currently 40 GHz, depends on the pulse duration and can be extended to over 0.8 THz [13, 14]. Coherent oscillations of P_S with delay are shown in Fig. 2(d). Here the switching probability peaks, always below $P_S=40\%$, decrease dramatically after 600 ps and disappear before 1000 ps.

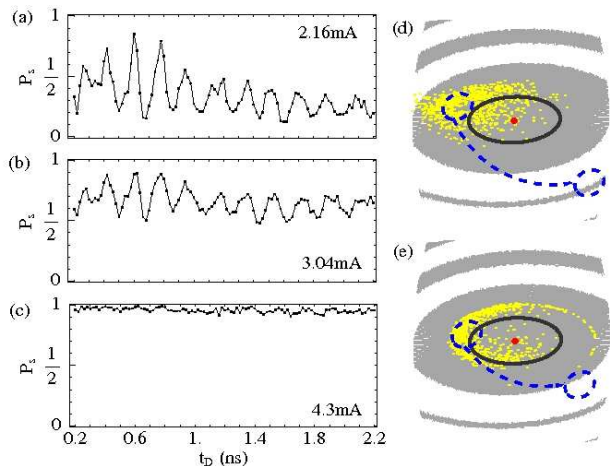


Figure 3: **5 ns pulse effective damping reduction** (a)-(c) P_S vs delay for 5 ns duration pulse amplitudes of (a) 2.16 mA, (b) 3.04 mA, and (c) 4.30 mA. (d), (e) Sections of the free layer moment phase portrait for the dotted region of Fig. 1(b), in the presence of a 1.2 mA 5 ns duration pulsed current. Yellow dots represent the \mathbf{m} ensemble just before the second ultrafast pulse for (d) $t_D=140$ ps and (e) $t_D=580$ ps. The solid dark line represents a stable orbit at 1.2mA while the blue (dashed) regions schematically represent regimes (i) and (ii) described in the text.

Since the nanomagnet effective damping can be modified via STT [4, 5], we apply dc currents to decrease the effective damping. For 0.6 mA dc current [Fig. 2(e)], we observe an additional peak at $t_D=1100$ ps, while the existing peak amplitudes (at 600, 780, and 940 ps) increase, indicating that the dc STT indeed reduces the damping. As for the zero dc current case, P_S decreases to 0% between successive peaks, demonstrating that a dc current alone does not contribute to switching. As the dc current increases to 1.6 mA [Fig. 2(f)] the peak amplitudes slightly increase but the peaks broaden substantially. This behavior can be explained with Fig. 2(c). At long times after applying a dc current sufficient to induce continuous precession (i.e. when the effective damping per cycle vanishes), the \mathbf{m} ensemble is distributed along a stable orbit (yellow), and thus the resulting \mathbf{m} ensemble after the first pulse (blue) is largely scattered in comparison to that obtained in the absence of dc currents. This scattering not only broadens the P_S oscillations but also explains why P_S no longer decreases to 0% between peaks for 1.6 mA currents. The dc current together with the first pulse displace some of the points into the white bands, inducing switching independently of the second pulse, yielding a nonzero P_S baseline.

To overcome the broadening and dephasing of trajectories in the \mathbf{m} ensemble that occur with dc currents, we employ instead a 25 ps risetime, 5 ns duration current pulse to reduce the effective damping. The first ultrafast pulse is precisely timed with the beginning of the 5 ns duration pulse throughout our measurements [see inset above Fig. 1(d)] and P_S is now measured vs. de-

lay for different 5 ns pulse amplitudes, I_{5ns} , as shown in Figs. 3(a)-(c). In every case I_{5ns} is greater than the “dc” switching current (measured using a sweep rate of 0.05 mA/s), and in sharp contrast with Figs. 2(e)-(f), Figs. 3(a)-(b) show P_S oscillations persisting out to our maximum delay, $t_D=2.2$ ns. For these 5 ns pulse data we observe three distinct P_S regimes: (i) below 0.6 ns, the P_S maxima are irregular and increase with increasing delay, (ii) between 0.6-1 ns the P_S oscillations monotonically decrease with increasing delay, and (iii) above 1 ns the oscillation amplitude is almost constant and shows a minimal decrease at longer t_D .

These three different regimes can be explained with the phase portrait sections in Figs. 3(d) and (e). An initial room temperature \mathbf{m} distribution equivalent to that in Fig. 2(a) evolves to the yellow dots shown in Figs. 3(d) and (e) for precession times of 0.14 ns and 0.58 ps respectively in the presence of a 1.2 mA, 5 ns pulse. At short times [Fig. 2(d)], the resulting \mathbf{m} distribution is close to the first gray-white switching boundary, whereas for longer precession times [Fig. 2(e)] the distribution has partially relaxed to the 1.2 mA stable orbit (dark line). The blue (dashed) ellipses and arrow schematically represent the evolution of a low temperature \mathbf{m} ensemble in response to the second ultrafast pulse. For short t_D the \mathbf{m} ensemble is displaced across various boundary crossings and the value of P_S depends on the particular phase portrait structure together with the shape of the thermal distribution, explaining the irregular behavior of P_S at short delays. As t_D increases the \mathbf{m} distribution before the second pulse moves towards the 1.2 mA stable orbit and the \mathbf{m} ensemble resulting from the second pulse is not pushed as far away from AP. For a particular value of t_D , here ~ 580 ps, the \mathbf{m} ensemble is mostly within the first white band, explaining the increase in P_S observed as t_D approaches 600 ps (regime i). As the delay continues to increase (regime ii), the \mathbf{m} distribution continues to relax towards the 1.2 mA stable orbit and thus P_S decreases monotonically. This relaxation occurs within 400 ps, a timescale set by the damping. When the \mathbf{m} distribution has almost reached the stable orbit, the amplitude of the P_S oscillations decreases at a much slower rate since the decay is now caused by “dephasing” and not by energy loss (regime iii). Therefore our data are consistent with complete damping cancellation over a range of currents. The dephasing of the trajectories corresponding to multiple repetitions of the experiment and resulting from the thermal distribution of initial orientations of \mathbf{m} can be observed in Fig. 3(e) (yellow dots). This dephasing will increase with t_D eventually leading to the complete dephasing shown by the yellow orbit in Fig. 2(c). As the amplitude of the 5 ns pulse increases, the stable orbit moves away from the AP stable point and the \mathbf{m} ensemble that results after the first ultrafast pulse is displaced across the first switching boundary, producing the background P_S observed in our measurements.

In our simulations and discussion we have ignored thermal effects on the magnetic moment motion. Thermal

fluctuations will introduce a stochastic component into the magnetization trajectories, broadening the \mathbf{m} distribution further [15]. This broadening can also contribute to the existence of a nonzero P_S background, and for long delays it will produce additional dephasing of the trajectories and eventually a disappearance of the P_S oscillations. By extending our technique to much longer times it should be possible to observe the dephasing of the ensemble of trajectories even though each trajectory on average does not lose any energy per precession cycle.

In conclusion, we demonstrate time domain detection of damping modification in a nanomagnet at room tem-

perature, and in contrast to dc currents, successfully achieve damping cancellation with a precisely-timed 5 ns pulse over a range of currents. In addition, our ultrafast time-domain measurement allows us to monitor the transient approach to an equilibrium precessional trajectory, where the damping cancellation and linewidth reduction seen in spin torque oscillators are established after a transient delay while the magnetization decays to the equilibrium orbit. These measurements suggest the possibility to further study thermal dephasing effects in oscillators, both while relaxing towards stable precession, and for times much longer than the precession period.

-
- [1] J. C. Slonczewski, *J. Magn. Magn. Mater.* **159**, L1 (1996).
 - [2] L. Berger, *Phys. Rev. B* **54**, 9353 (1996).
 - [3] D. Ralph and M. Stiles, *Journal of Magnetism and Magnetic Materials* **320**, 1190 (2008).
 - [4] I. N. Krivorotov, N. C. Emley, J. C. Sankey, S. I. Kiselev, D. C. Ralph, and R. A. Buhrman, *Science* **307**, 228 (2005).
 - [5] J. C. Sankey, P. M. Braganca, A. G. F. Garcia, I. N. Krivorotov, R. A. Buhrman, and D. C. Ralph, *Physical Review Letters* **96**, 227601 (2006).
 - [6] M. Tsoi, A. G. M. Jansen, J. Bass, W.-C. Chiang, M. Seck, V. Tsoi, and P. Wyder, *Phys. Rev. Lett.* **80**, 4281 (1998).
 - [7] J. A. Katine, F. J. Albert, R. A. Buhrman, E. B. Myers, and D. C. Ralph, *Phys. Rev. Lett.* **84**, 3149 (2000).
 - [8] J. C. Sankey, I. N. Krivorotov, S. I. Kiselev, P. M. Braganca, N. C. Emley, R. A. Buhrman, and D. C. Ralph, *Phys. Rev. B* **72**, 224427 (2005).
 - [9] D. Houssameddine, U. Ebels, B. Dieny, K. Garello, J.-P. Michel, B. Delaet, B. Viala, M.-C. Cyrille, J. A. Katine, and D. Mauri, *Physical Review Letters* **102**, 257202 (pages 4) (2009).
 - [10] J. Katine and E. E. Fullerton, *Journal of Magnetism and Magnetic Materials* **320**, 1217 (2008), ISSN 0304-8853.
 - [11] S. Garzon, L. Ye, R. A. Webb, T. M. Crawford, M. Covington, and S. Kaka, *Physical Review B (Condensed Matter and Materials Physics)* **78**, 180401 (2008).
 - [12] D. H. Auston, in *Picosecond Optoelectronic Devices*, edited by C. H. Lee (Academic, Orlando, 1984), pp. 73–117.
 - [13] T. Nagatsuma, T. Shibata, E. Sano, and A. Iwata, *Journal of Applied Physics* **66**, 4001 (1989).
 - [14] S. Verghese, N. Zamdmer, Q. Hu, and A. Förster, *Applied Physics Letters* **70**, 2644 (1997).
 - [15] W. F. Brown, *Phys. Rev.* **130**, 1677 (1963).